IDENTIFICATION OF UNMODELLED DYNAMICS IN A ROTOR-BEARING SYSTEM WITH BOUNDED UNCERTAINTY

Qingyu Wang and Eric H. Maslen
University of Virginia, ROMAC Laboratories
Department of Mechanical and Aerospace Engineering
122 Engineer's Way, Charlottesville, VA 22904 USA
qw4k@virginia.edu

ABSTRACT

In developing engineering models for rotating machine analysis, most of the components of the rotor–bearing–foundation system can be modelled relatively accurately. However, there are always some parts or interactions which are very hard to model, such as shrink fits or foundation components. Such parts or effects can be referred to as *unmodelled dynamics*.

This paper presents a non-parametric method to identify the unmodelled dynamics using the combination of an engineering model and experimental data. Assuming that errors in the engineering model and measurement noises are bounded, a bound is derived for the uncertainties in the identified dynamics by using μ-analysis. An illustrative example is given, and two widely used non-linear searching methods are compared to the $\mu-$analysis in estimating the bound, showing that the μ approach is the only efficient method to find a tight hard bound.

INTRODUCTION

Finite element models are widely used in rotordynamics analysis, and for a rotor-bearing system, most components can be modelled accurately. There are, however, some components such as shrink fits and foundation which may be hard to model due to a number of practical difficulties. Further, these parts or interconnections are often very hard to identify experimentally, because they cannot be measured directly: their tight integration in the overall system precludes direct access to their input/output. Therefore, they must be identified, if possible, together with the whole system.

There are two general approaches to model refinement or updating. The first approach assumes that the structure of the nominal engineering model is correct and seeks to modify specific parameters of the model to make the model I/O match the measured I/O. A good overview of this approach is provided by Friswel and Mottershead [1]. These methods assume there are errors in certain model parameters, such as stiffness or mass, and by comparing to the test data, these parameters can be adjusted. Usually these methods only improve the existing parameters of the engineering model, and the parameters usually cannot be frequency dependent. Therefore most of these methods may not be directly suitable for identifying unmodelled dynamics.

Recently, some researchers have begun to focus on frequency dependent problems, for instance, Sinha et al [4], who modelled the foundation from a single run-down of a machine. They assumed the foundation parameters are frequency dependent, then divided the frequency range into many bands, and applied model updating methods to each of them.

The second approach (Maslen et al [2]) assumes that the engineering model parameters are correct but that the model is completely missing certain dynamic elements whose model is completely unknown. All that is known about these missing elements is the manner in which they interact with the system described by the engineering model. The goal of model refinement here is to identify the simplest dynamic model of these missing elements that will cause the measurable dynamics of the resulting composite model to match those measured for the actual system.

These two approaches usually do not use the test data directly. They use a model of the data identified by black–box/system identification instead. The process can be represented by the diagram shown in Figure 1, where Box A and B forms a route to identify the unmodelled dynamics from the test data. Box A is the black-box type system identification, which identifies a model from test data. The test data can be both in time or frequency domain for system identification, but in this paper, only frequency response functions (FRFs) are used. Box B represents the model updating approaches, which use the identified model and the engineering model to improve certain parameters or identify the unmodelled dynamics.

This paper presents another route to identify the unmodelled dynamics from the test data, as indicated by the lower part of Figure 1. This route includes two boxes,

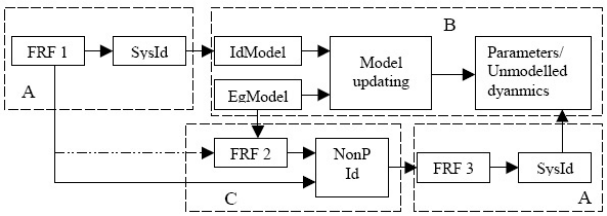

Figure 1: Identification diagram

Box C and also Box A, and Box C is the focus of this paper. In Box C, the non-parametric identification (NonP Id) requires FRF 1 and FRF 2, and generates FRF 3. FRF 1 is the test data in essentially raw (frequency response function) form. FRF 2 can be the either test data from the rest of the structure or generated from the engineering model, which will be explained later. FRF 3 is the FRF of the unmodelled dynamics. Notice that both routes use Box A, but in different positions. One advantage of the lower route is that, without begin tangled with the whole system, FRF 3 should be easier to identify. Another advantage is that it is possible to estimate the model quality of the unmodelled dynamics, and this is central to the objectives of this paper.

In the upper route, since the model updating approaches include the engineering model in the identification, the identified unmodelled dynamics may depend heavily on the quality of the engineering model, but very little literature has discussed how to estimate the influence of the errors of the engineering model, nor the influence of noise in the test data — the identified model is simply regarded as "true". Consequently, the uncertainty in the corrected model is only based on inability to fully match the data: the influence of model error on matching error is ignore. This generally produces a gross underestimate of uncertainty in the model corrections. Without a reliable bound on the uncertainty of the model corrections, it is essentially impossible to assess the accuracy of I/O projections other than those already measured: extrapolation from the data can't be done with any quantifiable uncertainty bounds. Hence, the corrected model is of very limited utility. We seek here to obtain a reliable bound on uncertainty of the model correction in order to ensure a reliable bound on model based extrapolative performance/response predictions.

Attention to this problem is increasing, particularly in the controls community. Some system identification methods have been presented that not only provide models but also provide bounds on the accuracy of those models ([3] and [5]), but all those methods require that the test data are bounded. This paper presents a method to bound FRF 3, so that those methods may be applied in deriving the model and the bounds.

CALCULATION OF THE UNMODELLED DYNAMICS

For the analysis of rotating machinery, it is most common to present a model in discrete (finite dimensional) form. The usual form of the model is:

$$M_0\ddot{x} + C_0\dot{x} + K_0 = f \tag{1}$$

where M_0, C_0 and K_0 are the mass, damping and stiffness matrices and f represents external loads or other effects such as mass unbalance. The Laplace transformation of the above equations is:

$$Z_0 x = F \tag{2}$$

where $Z_0 = s^2 M_0 + sC_0 + K_0$ is the dynamics stiffness matrix. The dimension of Z_0 is related to the number of lumped mass stations along the shaft. Each element in Z_0 corresponds to certain location on the shaft in certain coordinate, while each location on the shaft may correspond to several elements in Z_0. To select specific locations on the shaft, two location matrices $[T_a]_{n\times a}$ and $[T_b]_{n\times b}$ can be introduced. The elements in Z_0 corresponding to these locations are $E_{a\times b} = T_a^T Z_0 T_b$. Conversely, if some additional dynamic system, $\hat{E}$, is connected to these locations, Z_0 can be simply corrected as $Z_1 = Z_0 + T_a \hat{E} T_b^T$.

Consider the FRF data of an experiment: only several locations are excited and/or sampled. Let T_e and T_s be the input and output location matrices so that the I/O relation is:

$$Z_0 x = T_e F_e \tag{3}$$

$$z = T_s^T x \tag{4}$$

or simply $z = T_s^T Z_0^{-1} T_e F_e$, where F_e are the excitation forces. Assume that the unmodelled dynamics, denoted as $D_u(s)$, occur at locations T_u so that the true transfer function from F_e to z becomes

$$P_1 = T_s^T (Z_0(s) + T_u(-D_u(s))T_u^T)^{-1} T_e \tag{5}$$

By using the matrix inversion formula [6], (5) can be rewritten as

$$P_1(s) = G_{11} + G_{12}(I - D_u(s)G_{22})^{-1} D_u(s) G_{21} \tag{6}$$

where

$$\begin{aligned} G_{11}(s) &= T_s^T Z_0^{-1} T_e \\ G_{12}(s) &= T_s^T Z_0^{-1} T_u \\ G_{21}(s) &= T_u^T Z_0^{-1} T_e \\ G_{22}(s) &= T_u^T Z_0^{-1} T_u \end{aligned}$$

$D_u(s)$ can be calculated from (6) as

$$D_u(s) = -(G_{21}(G_{11} - P_1)^{-1} G_{12} - G_{22})^{-1} \tag{7}$$

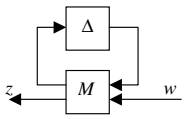

Figure 2: Analysis Framework

If G_{12} and G_{21} are square and full rank, i.e. there are as many excitations and sensors as there are connections to the unmodelled dynamics, the required inverses will exist; otherwise, the direct inversion will not be possible. Due to signal noise in real data, the inversion is often possible despite this, but the resulting predictions will be extremely noisy with uncertainties that cannot be bounded.

μ-ANALYSIS

μ-analysis is a powerful tool in robust control, and this paper is a mechanical engineering application of this tool. μ-analysis will be only introduced briefly in this section: see [6] for a more complete description of the method.

Figure 2 shows the general framework of μ-analysis, where

$$z = \mathcal{F}_u(M, \Delta)w \tag{8}$$

M is a complex matrix partitioned as

$$M = \begin{bmatrix} M_{11} & M_{12} \\ M_{21} & M_{22} \end{bmatrix} \tag{9}$$

Δ is defined as

$$\Delta = diag[\delta_1 I_{r1}, ..., \delta_s I_{rs}, \Delta_1, ..., \Delta_F] \tag{10}$$

where $I_{r,i}$ are identity matrices, and δ_i / Δ_i are unknown but bounded complex numbers/matrices. $\mathcal{F}(M, \Delta)$ is an upper link linear fractional transformation (LFT), defined as

$$\mathcal{F}_u(M, \Delta) = M_{22} + M_{21}\Delta(I - M_{11}\Delta)^{-1}M_{12} \tag{11}$$

Most model uncertainty can be represented in this form. Consider a simple situation that $\mathcal{F}_u(M, \Delta)$ is 1-by-1, i.e. a complex number, and M is a constant complex matrix. Because Δ is uncertain, $\mathcal{F}_u(M, \Delta)$ is a cloud (ball) of possible complex numbers. μ-analysis finds a bound for the size of this cloud. Let

$$\gamma_t = \max_{\Delta} |\mathcal{F}_u(M, \Delta)|$$

then γ_t is the true/tightest bound of this cloud measured from the origin. To find γ_t is the same as to find the global minimum of a non-linear function, which is a very hard problem. μ-analysis derives an over-bound γ_o, an under-bound γ_u, and a worst-case Δ_w (a constant complex matrix within the uncertainty range), such that $\gamma_u \leq \gamma_t \leq \gamma_o$ and $\gamma_u = |\mathcal{F}_u(M, \Delta_w)|$. Notice that $\mathcal{F}_u(M, \Delta_w)$ is a actual point on the edge of the cloud, and γ_u is achievable.

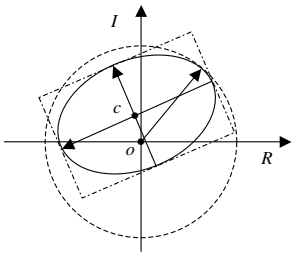

Figure 3: The uncertainty cloud and the bounds

This over– under–bound strategy avoids directly searching for the global minimum, and the searching can be finished in polynomial time. Further, the two bounds are very close for most systems [6] so the pair of bounds is useful. γ_o can be used as the bound, and γ_u can be used to calculate a boundary tightness indication (BTI) to show how conservative γ_o is:

$$\text{BTI} \equiv \gamma_u/\gamma_o \tag{12}$$

The closer BTI is to 1, the closer γ_o is to γ_t.

γ_t can be seen as the furthest distance between the origin and all points in the cloud. Due to the shape of the cloud, γ_t may not be the best way to describe the cloud, which can be illustrated by Figure 3. The radius is γ_t and the solid-line ellipsoid represents the cloud. Another way to describe the cloud is to give the center c and the two principle components of the rectangular box. This can be done by moving the origin several times to get several points on the edge of the cloud. Usually the rectangular box is smaller than the circle.

CALCULATION OF THE BOUND

There are several kinds of uncertainty present in the engineering model and test data, such as errors in the engineering model introduced in the process of the discretization and measurement noises of the sensors. Therefore all the transfer functions at the right side of Equation 7 have uncertainties. This section will transform these uncertainties and the transfer functions in Equation 7 into the form introduced in last section, and then apply μ-analysis to derive the bound.

The first step is to add uncertainties to both sides of Equation 7. Let $\hat{D}_u$ be the unmodelled dynamics with uncertainty, then $\Delta_d = D_u - \hat{D}_u$ is the uncertainty, and it can be derived trivially from (7) as:

$$\Delta_d = D_u + \hat{G}_{12}^{-1}(\hat{G}_{11} - \hat{P}_1)\times \\ \times(I - \hat{G}_{21}^{-1}\hat{G}_{22}\hat{G}_{12}^{-1}(\hat{G}_{11} - \hat{P}_1))^{-1}\hat{G}_{21}^{-1} \tag{13}$$

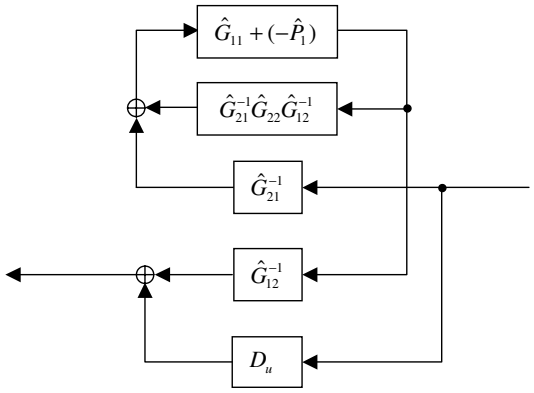

Figure 4: System diagram 1

in which the hatted symbols are uncertain. The objective is to bound Δ_d. The system diagram is shown in Figure 4.

The next step is to build uncertainty bounds for each transfer function shown in Figure 4. For P_1, an ensemble of experiments can be conducted and the resulting scatter in each data point can be assessed as an uncertainty bound. For $G_{ij}, i, j = 1, 2$, experiments are preferred if possible, and the bounds can be built as for P_1. Sometimes it is not possible to do the experiments without the unmodelled dynamics components being involved, like the foundation. In this case, the uncertainties of M_0, C_0 and K_0 should be estimated by engineers.Either way, each transfer functions can be expressed as a known transfer function with bounded uncertainty. Figure 5 shows the system diagram, where $\widetilde{G}_{ij}, i, j = 1, 2$ have different expressions according to different approaches to obtaining the bounds.

The third step is to pull individual uncertainty matrices out and rearrange the model into the standard μ-analysis form. The diagram is shown in Figure 6.

The last step is to use μ analysis to get the bound for Δ_d. If Δ_d is only a complex number, then the method introduced in last section can be applied directly. Otherwise, each element can be bounded separately. The bound can be simply the radius of the circle, or a rectangular box (the center and two principle components).

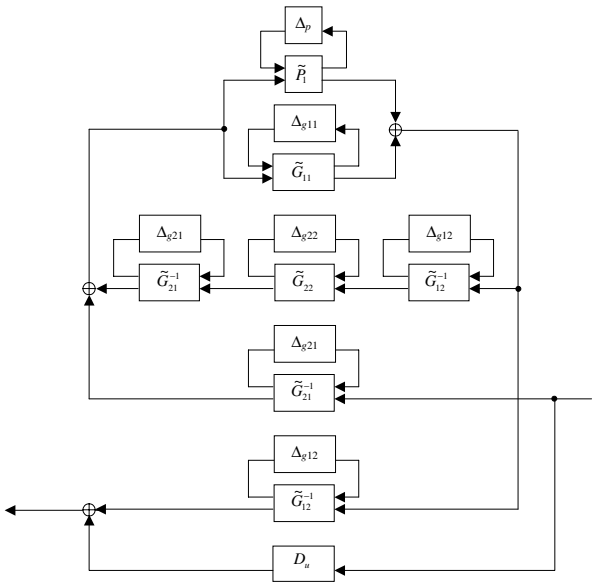

Figure 5: System diagram 2

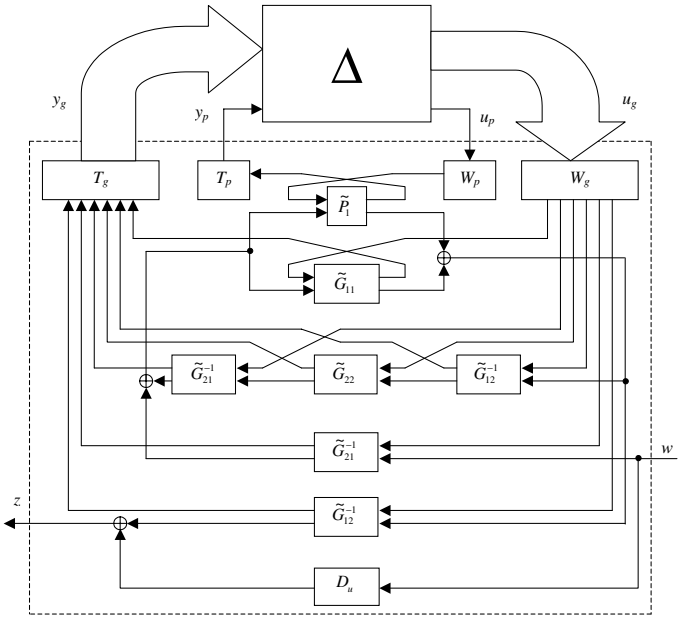

Figure 6: System diagram 3

A SIMULATION EXAMPLE

The Engineering Model and Test Data

Figure 7 shows a simplified rotor-foundation system, where $M_r = 20$ kg, $M_f = 100$ kg, $C_b = 1000$ Ns/m, $C_f = 100$ Ns/m, $K_b = 10^5$ N/m and $K_f = 10^6$ N/m. For the engineering model, M_f, C_f and K_f are not known, and estimated values of $M_g = 50$ kg, $C_g = 200$ Ns/m and $K_g = 3 \times 10^6$ N/m are used instead. The

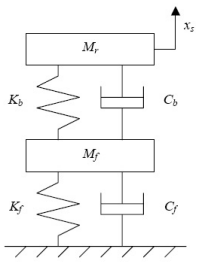

Figure 7: Simplified rotor-bearing-foundation system

engineering model is:

$$\begin{aligned} M_0 &= \begin{bmatrix} M_g & 0 \\ 0 & M_r \end{bmatrix} \\ C_0 &= \begin{bmatrix} C_g - C_b & -C_b \\ -C_b & C_b \end{bmatrix} \\ K_0 &= \begin{bmatrix} K_g - K_b & -K_b \\ -K_b & K_b \end{bmatrix} \\ T_u &= \begin{bmatrix} 1 & 0 \end{bmatrix}^T \\ T_e &= T_s = \begin{bmatrix} 0 & 1 \end{bmatrix}^T \end{aligned}$$

with eigenfrequencies of 70.11 and 247.02 rad/s. The true plant is:

$$\begin{aligned} M_1 &= \begin{bmatrix} M_g & 0 \\ 0 & M_r \end{bmatrix} + \Delta_m \\ C_1 &= \begin{bmatrix} C_g - C_b & -C_b \\ -C_b & C_b \end{bmatrix} + \Delta_c \\ K_1 &= \begin{bmatrix} K_g - K_b & -K_b \\ -K_b & K_b \end{bmatrix} + \Delta_k \end{aligned}$$

where

$$\Delta_m = 0.01 \begin{bmatrix} m_{11}\delta_{11} & m_{12}\delta_{12} \\ m_{21}\delta_{21} & m_{22}\delta_{22} \end{bmatrix}$$

and $|\delta_{ij}| \leq 1$,$i, j = 1, 2$ is a real uncertainty. Δ_c and Δ_k are defined similarly and also represent 1% uncertainties. The eigenfrequencies of the real system are 69.61 and 102.13 rad/s.

The FRF data are generated as:

$$P_1(s) = T_s^T(s^2M_1 + sC_0 + K_1)^{-1}T_e(1 + 0.02\delta_p)$$

where $|\delta_p| < 1$ is a complex uncertainty, and $s = j\omega, \omega \in [0.2\pi, 40\pi]$.

Non-linear Minimization (NM) and Random Search (RS)

Non-linear minimization (NM) and random search (RS) are widely use for non-linear problems. They are compared to μ-analysis (MU) in this example.

In Random Search (RS), the unmodelled dynamics together with the uncertainty can be expressed as a non-linear function of the model, FRF data and their uncertainties:

$$\hat{D}_u(s) = f(\Delta, Z_0, P_1) \tag{14}$$

For each frequency point, by randomly assign Δ certain values within the range, a set of $\hat{D}_u$ can be calculated. The edge of the set can be picked out as the bound. The bigger the size of the set, the closer the bound is to the true one.

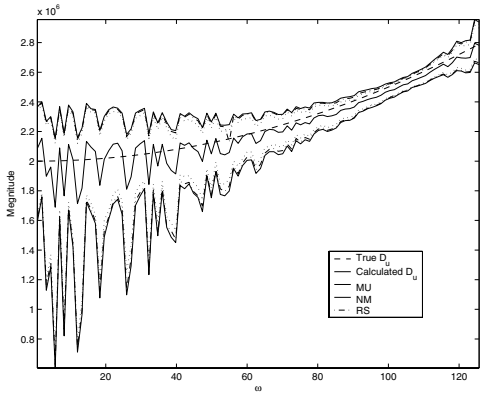

Figure 8: Uncertainty bound

In Nonlinear minimization (NM), the Δ in Equation 14 can be regarded as variables with constraints. This kind of problem can be solved using any of several well developed non-linear minimization tools. A rectangular box for the uncertainties can be obtained similar to that obtained through μ-analysis. The initial value of Δ has a strong influence on the result.

The Results

For RS, 10000 $\hat{D}_u$ were calculated for each frequency point. For NM, the initial value of $\Delta_0 = 0$ was used. Figure 8 shows the calculated $|D_u|$, the true $|D_u|$, $\max|\hat{D}_u|$ and $\min|\hat{D}_u|$. This figure gives only a big picture that D_u is contained in all the bounds and the MU bounds contain everything. The bound is rather big for some frequencies considering only 2% uncertainties added, e.g., the lower bound at $\omega = 5$ rad/s almost reaches 0 and the upper bound is about 2.4×10^6 N/m.

To compare the three methods clearly, normalized upper bounds ($\max|\hat{D}_u| - |D_u|$)s are shown in Figure 9, where the MU upper bound is 1. The average value, minimum value and calculation time are shown in Table 1. The BTI shows that MU is very close to the true bound. NM is closer to MU on average than RS, but there is a sharp peak at $\omega = 55$ rad/s. This problem can be solved by using different Δ_0s, but the calculation time will be accordingly longer. For instance, if 20 randomly chosen Δ_0 are used, then the minimum value becomes 0.838, the average value is 0.929, and the calculation time is 385 seconds. The minimum value is much better, but the average value shows very little improvement.

Figure 10 shows the complex plane at a randomly picked frequency $\omega = 37.25$ rad/s, where the rectangular boxes of MU and NM are shown, and the RS set of $\hat{D}_u$ are used directly as the cloud inside the boxes. The star on the right side of the inner MU bound is an achievable point. The MU boxes contain the cloud but not the whole NM box, because the simple shape of a rectangu-

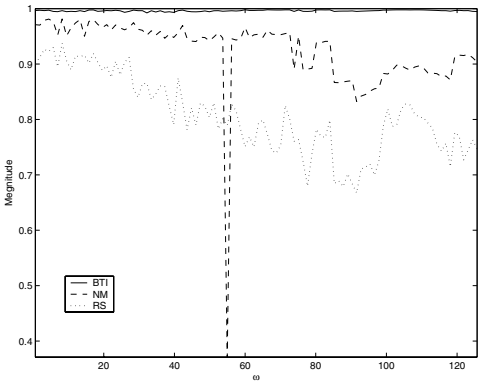

Figure 9: Normalized uncertainty upper bounds

Method	Time (s)	Average Value	Min Value
MU	218	1	1
BTI	NA	0.996	0.992
NM	18.5	0.924	0.371
RS	434	0.806	0.667

Table 1: Upper Bound Comparison

lar box brings in non-achievable points, which can also be seen from Figure 3. This figure shows that, even if 10000 iterations are used in RS, the edge of the cloud is still far from the achievable point. More importantly, without MU, it is hard to know how close it is.

DISCUSSION AND CONCLUSION

This paper presents a non-parametric method to identify unmodelled dynamics along with a very tight bound on the uncertainty of the extracted model. The calculation of the unmodelled dynamics is simple and straightforward, given experimental data (and the engineering model). Since there are various uncertainties in the engineering model and test data, the quality of calculated unmodelled dynamics are estimated. Two general methods are compared in searching for the bound in the example. These two methods usually cannot find the exact bound in limited time if there are certain number of uncertainties, such as 10. For LFT form uncertainties, the μ-analysis can derive a narrow interval containing the exact bound, and the example shows how narrow the interval typically is.

Although the MU bound is very close the the "tightest" bound, there are at least three problems which may make the "tightest" bound conservative: a) The uncertainties of the engineering model may have some interconnections, such as the density error could affect all parts of M_0. b) The uncertainties for each frequency points are assumed to be independent, but actually they may not be. c) When D_u is not 1-by-1, each element is bounded separately, which can also bring in conservativeness. These problems are not considered in this paper, but they need to be kept in mind when MU (or any other uncertainty estimation technique) is used.

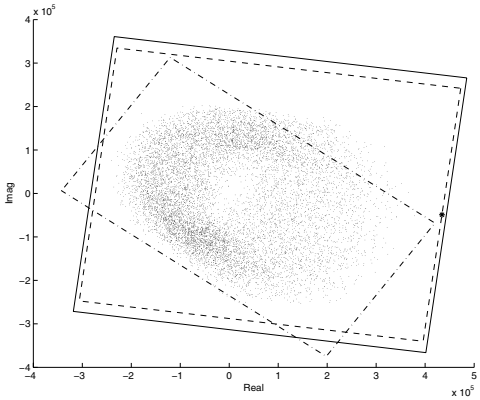

Figure 10: Uncertainty bounds for $\omega = 37.25$ rad/s, where – Outer bound of MU, - - Inner bound of MU,-· - NM

The results — FRFs of D_u and the bounds for each frequency point — can be used directly, such as to derive the system performance FRFs, or a parametric model can be identified from them. A simple way to identify the parametric model is to curve fit the FRFs and check if the fitted result is inside the bounds. More sophisticated identification methods can be found in the literature such as [3] and [5].

REFERENCES

[1] M. I. Friswell and J. E. Mottershead, Finite Element Model Updating in Structural Dynamics, 1995

[2] Eric H. Maslen, Jose A. Vazquez and Christopher K. Sortore, Reconciliation of Rotordynamic Models with Experimental Data, Journal of Engineering for Gas Turbines and Power, Vol. 124 No. 2 2002 Apr pp. 351-356

[3] M. Milanese and A. Vicino, Optimal Estimation Theory for Dynamic Systems with Set Membership Uncertainty: An Overview, Automatica, Vol. 27, No. 6, 1991, pp. 997-1009

[4] J. K. Sinha, M. I. Friswell and A. W. Lees, The identification of the Unbalance and the Foundation Model of A Flexible Rotating Machine From A Single Run-Down, Mechanical Systems and Signal Processing, Vol. 16, No. 2-3, pp. 255-271

[5] Eric Walter and Helene Piet-lahanier, Estimation of Parameter Bounds from Bounded-Error Data: A Survey, Mathematics and Computers in Simulation, Vol. 32, 1990, pp. 449-468

[6] Kemin Zhou, John C. Doyle and Keith Glover, *Robust and Optimal Control* 1995